

Improving Yttrium-90 PET scan image quality through optimized reconstruction algorithms

Pei Ing Ngam^{1,2}, Eelin Tan³, Gabriel Lim¹, Sean Xuexian Yan¹

¹Department of Nuclear Medicine and Molecular Imaging, Singapore General Hospital

²Department of Diagnostic Imaging, National University Hospital, Singapore

³SingHealth Radiological Sciences Academic Clinical Programme, Singapore General Hospital

Corresponding Author: Sean Xuexian Yan

Position: Senior Consultant; Associate Professor

Affiliation: Department of Nuclear Medicine and Molecular Imaging, Singapore General Hospital

Address: Outram Road, Singapore 169608

Phone: (+65) 63266040

Fax: (+65) 62240938

Email: sean.yan.x.x@singhealth.com.sg

First Author: Pei Ing Ngam

Position: Associate Consultant

Affiliations: Department of Diagnostic Imaging, National University Hospital and Department of Nuclear Medicine and Molecular Imaging, Singapore General Hospital

Address: 5 Lower Kent Ridge Rd, Singapore 119074

Phone: (+65) 67795555

Fax: (+65) 67797101

Email: pei_ing_ngam@nuhs.edu.sg

Manuscript word count: 3673 words

Disclosure: No conflict of interest relevant to this article was reported

ABSTRACT

The study aimed to improve the quality of the 90Y PET imaging by optimizing the reconstruction algorithm. **Methods:** Ten patients with metastatic neuroendocrine tumour to the liver or primary hepatocellular carcinoma who were qualified for 90Y labelled selective internal radiation therapy (SIRT) or peptide receptor radionuclide therapy (PRRT) were recruited. They underwent post-therapy PET/CT imaging using three different reconstruction parameters: (Algorithm A)Vue Point HD with 6.4mm filter cutoff, 24 subsets and 2 iterations, (Algorithm B)Vue Point FX with 6.0 mm filter cutoff, 18 subsets and 3 iterations using time of flight, and (Algorithm C)Vue Point HD LKYG with 5mm filter cutoff, 32 subsets and 1 iteration. The reconstructed PET/CT images were assessed by 10 nuclear medicine physicians using 4-point semi-qualitative scoring criteria. A P-value of less than 0.05 was considered significant. **Results:** The median quality assessment scores for Algorithm C were consistently scored the highest with algorithms A, B and C scoring 3, 2 and 4 respectively. The 90Y PET scans using Algorithm C were deemed diagnostic 91% of the time. There was a statistically significant difference in quality assessment scores between the algorithms by the Kruskal-Wallis rank sum test ($\chi^2(2) = 86.5$, $p < 0.001$), with mean rank quality score (QS) of 130.03 for Algorithm A, 109.76 for Algorithm B and 211.71 for Algorithm C. Subgroup analysis for quality assessment score of post-PRRT imaging alone showed statistically significant difference between different scanning algorithms ($\chi^2(2) = 35.35$, $p < 0.001$), with mean rank QS of 45.85 for Algorithm A, 50.05 for Algorithm B and 85.6 for Algorithm C. Similar results were observed for quality assessment score of post-SIRT imaging ($\chi^2(2) = 79.90$, $p < 0.001$), with mean rank of 82.33 for Algorithm A, 55.79 for Algorithm B and 133.38 for Algorithm C. **Conclusion:** The new LKYG algorithm that was featured by decreasing the number of iterations, decreasing the cutoff of the filter thickness, and increasing the number of the subsets had successfully improved the image quality.

Keywords: reconstruction algorithms, image quality, 90Y PET, SIRT, PRRT

INTRODUCTION

Yttrium-90 (^{90}Y) is one of the most commonly used radionuclides in contemporary Nuclear Medicine as both diagnostic and therapeutic agent, giving rise to lauded concept of Theranostic. This is owing to its outstanding physical and chemical features (1). ^{90}Y based radiopharmaceuticals have been utilized in various oncologic therapies, which includes but not limited to ^{90}Y -labelled anti-CD20 monoclonal antibody (Zevalin) radioimmunotherapy for lymphoma, ^{90}Y -dotapeptide radionuclide therapy for neuroendocrine tumors, and ^{90}Y -microspheres selective radiation therapy (SIRT) for liver tumors (2). Post-therapy imaging is therefore essential in confirming successful delivery of ^{90}Y labelled agent, dosimetry of the tumor(s) and critical organs, and dose planning for next treatment.

The conventional post-imaging modality using ^{90}Y Bremsstrahlung technique unfortunately bears hereditary drawbacks of poor spatial resolution and unsatisfactory readability. ^{90}Y PET/CT on the other hand has emerged as the modality of choice for better quality of the post-therapy scan. Despite the advancement in technology, the main challenge for ^{90}Y PET imaging is its extremely low abundance of positron emission per decay that requires long scanning time for adequate signal to noise ratio. Due to patient's general intolerability of prolonged scan time, it is very difficult to achieve adequate counts and the quality of PET image has been reported unsatisfactory in many literatures, with standard or modified reconstruction algorithm. There is also lack of consensus guidelines for the technical acquisition, imaging reconstruction, and qualitative/quantitative interpretation of ^{90}Y planar, SPECT and PET imaging. In addition, the vast majority of nuclear medicine imaging systems are not currently designed or specifically optimized for ^{90}Y imaging applications (3).

In this article, we report our efforts in modifying the reconstruction algorithm and consequent improvement of ^{90}Y PET imaging quality in order for our experience to serve as a reference for other practitioners.

METHODS AND MATERIALS

Study Cohort

A total of 10 consecutive patients qualified for ^{90}Y labelled selective internal radiation therapy (SIRT) or peptide receptor radionuclide therapy (PRRT) were recruited. For ^{90}Y -PRRT, the ^{90}Y was purchased from Perkin Elmer (Waltham, Massachusetts, United States) and the ^{90}Y -DOTATATE was then synthesized in our department's radiopharmacy. ^{90}Y -DOTATATE with the dose ranging from 3.0 to 5.0 GBq were given intravenously to the patients in the dedicated isolation ward. For ^{90}Y -SIRT, ^{90}Y microspheres were purchased from SIRTEX Medical Singapore Pte. Ltd. (Singapore). ^{90}Y microspheres with the dose ranging from 0.5 to 3.0 GBq were administered intra-arterially to the targeted hepatic lesion(s) in interventional radiology suite in Singapore general hospital.

Scanning Protocol and Reconstruction Algorithm

All patients were then scanned on GE 690 Discovery PET/CT scanner either on the same day or the next morning. A low-dose CT protocol at 120 kV, automated mA ranging between 10mA and 200mA current modulation, and a noise index of 18 was obtained for attenuation correction and anatomic localization purposes followed by PET acquisition for 30 minutes per bed position, covering from the diaphragm to the iliac crest of the pelvis for SIRT patients and variable locations for PRRT patients depending on where disease burden is. PET images were corrected for motion and attenuation on the basis of the CT data. The reconstruction was performed using both fully 3-dimensional ordered subset expectation maximization (OSEM) algorithm either with or without time of flight (TOF), and GE sharp IR point-spread function algorithm. Three different reconstruction parameters with variation of full width at half maximum (FWHM) Gaussian filter size as well as number of iterations and subsets (Table 1) are namely: (Algorithm A) Vue Point HD (VPHD: non-TOF) with 6.4mm filter cutoff, 24 subsets and 2 iterations; (Algorithm B) Vue Point FX (VPFX: with TOF) with 6.0 mm filter cutoff, 18 subsets and 3 iterations; (Algorithm C) VPHD LKYG (non-TOF) with 5mm filter cutoff, 32 subsets and 1 iteration. The reconstructed matrix size was 192 x 192 with a pixels dimension of 3.65 mm. Algorithms A and B were routinely used in our center and many other centers while algorithm C was purposefully modified and named LKYG. Maximum intensity

projection images were also generated. Both attenuation corrected and uncorrected PET images as well as PET/CT fusion images were reviewed.

Quality Assessment

For each patient, the reconstructed PET/CT images using three different algorithms were presented to 10 nuclear medicine physicians (readers) with working experience ranges from 2 to 20 years for quality assessment. The quality of images was graded according to the semi-qualitative scoring criteria as non-diagnostic, barely diagnostic, fairly diagnostic and excellent diagnostic (Table 2). All readers are blinded to the reconstruction algorithms.

Statistical Analysis

Statistical quality assessment scores comparison was made between each algorithm by non-parametric Kruskal-Wallis rank sum test and post-hoc Wilcoxon rank sum in the event of a statistically significant difference in the Kruskal Wallis test. The potential confounding factors including age, gender, body mass index (BMI), types of radioligand and dose were examined with multivariable ordered logistic regression analysis. Statistically significant threshold (P-value) was set at 0.05. Ordinal and continuous variables are reported in median values with interquartile range (IQR). Results from ordered logistic regression analysis are reported in odds ratios (OR) with corresponding 95% confidence intervals (95% CI). Interrater reliability was assessed with mixed-effects intraclass correlation coefficient (ICC), whereby ICC below 0.5 constitutes poor interrater agreement, ICC between 0.5 and 0.75 constitutes moderate interrater agreement, ICC between 0.75 and 0.9 constituting good interrater agreement and ICC above 0.9 constituting excellent interrater agreement.

Statistical analysis was conducted on RStudio (R version 3.6.3, R Foundation for Statistical Computing, Vienna, Austria).

RESULTS

Patient demographics and PET study parameters

Ten patients including 8 males and 2 females, with a mean age of 61.5 ± 17.3 years, and a mean BMI of 23.54 ± 3.49 kg/m² were recruited into our study (Table 3). Four patients including 1 patient with rectal NET, 2 patients with midgut NET and 1 patient with paraganglioma received a mean 90Y PRRT dose of 3.66Gbpq. Six patients include 5 patients with HCC and 1 patient with metastatic pancreatic NET to liver received a mean 90Y SIRT dose of 1.85Gbpq.

Interrater reliability

The interrater reliability for the readers was found to be moderate to good with Kappa of 0.82 ($p < 0.001$), 95% CI (0.66,0.93) for algorithm A, 0.625 ($p < 0.005$), 95% CI (0.29,0.85) for algorithm B, and 0.502 ($p < 0.05$), 95% CI (0.06,0.80) for algorithm C.

Quality assessment scores

The median quality assessment scores for algorithms A, B and C were 3 (IQR 1), 2 (IQR 1), 4 (IQR 1), respectively (Figure 1). Algorithm C consistently scored the highest for each patient compared to Algorithm A and B. Ninety-one percent of the time, the post-SIRT or post-PRRT scans using Algorithm C were deemed diagnostic (QS-3 and QS-4) by the 10 readers, achieving QS-4 53% of the time and QS-3 39% of the time. Only 1% of the time, Algorithm C was not diagnostic compared to that of 10% of the time for Algorithm A and 14% for Algorithm B.

There was a statistically significant difference in quality assessment scores between the algorithms by the Kruskal-Wallis rank sum test ($\chi^2(2) = 86.5$, $p < 0.001$) (Table 4), with mean rank quality score (QS) of 130.03 for Algorithm A, 109.76 for Algorithm B and 211.71 for Algorithm C. Post hoc Wilcoxon rank sum test showed that algorithm C scored significantly higher compared to algorithms A and B (A vs C, $p < 0.001$; B vs C, $p < 0.001$), whereas there was no significant difference between quality assessment scores between algorithms A and B (A vs B, $p = 0.064$).

Subgroup analysis for quality assessment score of post-PRRT imaging alone showed statistically significant difference between different scanning algorithms as well ($\chi^2(2) = 35.35$, $p < 0.001$), with mean rank QS of 45.85 for Algorithm A, 50.05 for Algorithm B and 85.6 for Algorithm C. Similar results were observed for quality assessment score of post-SIRT imaging ($\chi^2(2) = 79.90$, $p < 0.001$), with mean rank of 82.33 for Algorithm A, 55.79 for Algorithm B and 133.38 for Algorithm C. Therefore, we concluded Algorithm C remained out performing Algorithm A and Algorithm B for both post-SIRT therapy and post-PRRT scans. For post-SIRT therapy scans, Algorithm C fared remarkably better with a minimum scoring of QS-3 and achieved excellent scoring of QS-4 75% of the time. For post-PRRT PET scans, algorithm C again fared remarkably better achieving a good score of either QS-3 or QS-4 77.5% of the time compared to 15% for Algorithm A and 32.5% for Algorithm B.

The Wilcoxon Signed-Rank test showed that the imaging quality of post-SIRT therapy scans (mean rank = 65.3 for Algorithm A, 58.26 for Algorithm B, and 63.13 for Algorithm C) was constantly better than the imaging quality of post-PRRT scans regardless of the types of algorithms used (mean rank = 28.3 for Algorithm A, 38.86 for Algorithm B, and 31.56 for Algorithm C), [$Z = -6.70$, $p < 0.001$ for Algorithm A, $Z = -3.54$, $p < 0.001$ for Algorithm B, and $Z = -5.96$, $p < 0.001$ for Algorithm C)].

We present a case example of a patient with metastatic rectal neuroendocrine tumour to the liver (Figure 2). The SUVmax values for the dominant lesion in left hepatic lobe measures 47.7, 34.0 and 33.7 for Algorithm A, B and C respectively while the SUVmax values for the dominant lesion in the right hepatic lobe measures 33.9, 35.2 and 22.8 for Algorithm A, B and C respectively. Overall, Algorithm C demonstrated outstanding diagnostic yield with excellent signal-to-noise ratio compared to that of Algorithm B and C.

Confounding factors

Results from multivariable ordered logistic regression analysis are summarized in Table 5. Age, BMI and type of radiotracers were found to be the confounding factors. Younger age (adjusted OR, 0.98, 95% CI, 0.95-0.997) and lower BMI (adjusted OR, 0.90, 95% CI, 0.81-0.99) were associated with better quality assessment scores. SIRT was associated with significantly higher scores compared to PRRT (adjusted

OR, 23.99, 95% CI, 11.87-50.35). Additionally, the multivariable model also confirmed that quality assessment scores for algorithm C were significantly higher (adjusted OR, 17.4, 95% CI, 9.16-34.15). On the multivariable model, algorithm B performed significantly worse compared to algorithm A (adjusted OR, 0.46, 95% CI, 0.26-0.80).

DISCUSSION

^{90}Y is the commonly used theranostics agent for personalized patient treatment owing to its excellent physical and chemical features (1) optimal half-life of 64.1 hours, which is both long enough to allow relative ease in shipping and delivery, and short enough to achieve a critical dosing rate in tumour tissue, (2) high specific activity with relatively longer soft tissue penetration (mean 2.5mm) allows effective treatment with high cross-fire effect, and (3) pure β^- -emitter, which results in low radiation exposure to the medical staff and family members and therefore allows its application in outpatient setting.

Absence of gamma photon emission of ^{90}Y however significantly limits its utility as post-therapy imaging and dosimetry. Bremsstrahlung imaging and positron emission tomography (PET) scan on the other hand are commonly used for post-therapy localization and dosimetry of ^{90}Y labelled agents.

^{90}Y bremsstrahlung photons that are generated from the interaction between the β^- particle and matter allows imaging of these photons using gamma camera (4). This imaging technique is easily available but bears hereditary drawbacks of poor resolution of scintigraphy thus poor localization of biodistribution and inaccurate dosimetry of the tumor. This is attributed by a wide range of photon energies produced, internal photon scattering, variable count rates, low spatial resolution, and difficulty with selection of collimation and overlying tissue attenuation.

While the branching ratio for internal pair-production is very small at approximately 32 per million decays, ^{90}Y PET/CT imaging shows better spatial resolution and contrast and thus higher detection rate compared to the traditionally used bremsstrahlung imaging in numerous phantoms and clinical studies (5,6). Interestingly, Kao et al. recently demonstrated feasibility of ^{90}Y PET for quantitative assessment of residual activity in the delivery apparatus compared the conventional indirect method recommended by

manufacturer (7). The inherent problem is the low percentage of internal pair-production requires unrealistically long acquisition time for adequate signal to noise ratio. In real world, imaging time of 30 minutes per bed position would be the maximum achievable target for the patient to hold still. Any longer scan time is strongly not recommended as movement by the patient will result in un-sharpness of the image.

Various 90Y PET imaging techniques with or without TOF and resolution recovery capabilities as well as on semiconductor based scanners have shown potential resolution and contrast superior to bremsstrahlung single photon emission computed tomography (SPECT) (8,9). Despite multiple in vitro and in vivo studies on various PET imaging systems, acquisition times and different reconstruction algorithms, there is no standardized imaging protocol thus far although some manufacturers have provided technical support (10). Using our routinely used algorithms, PET images are usually of poor quality despite increasing the acquisition time. The low signal to noise ratio makes the tumor uptake quite often indistinguishable from background uptake.

Our team explored different reconstruction algorithms by formulating the filter dynamics for reconstruction in PET Imaging. We noticed that the sharpness and resolution of the image improved with increased number of iterations and subsets. This however also increases noise. Therefore, striking the right balance of signal to noise ratio is key to any filter algorithm. Our team subsequently set off for sharp reduction in the number of iterations and thus resulting in considerable noise reduction. In addition, we reduced the filter cutoff to 5mm aiming for a more stringent signal bandwidth and increased number of subsets to enhance sharpness. After multiple attempts in adjusting the settings and fine-tuning the parameters, we finally settled LKYG algorithm which is of significantly lower number of iterations, thinner filter cutoff and larger number of subsets as compared to our conventional algorithm. The strength of this combination is well demonstrated by the achieved, significantly improved image quality.

Our study is limited by small cohort and hence analysis of the confounding factors is limited. A semiquantitative scoring allows room for variation and hence a quantitative scoring will be preferred for more objective assessment.

CONCLUSION

Optimization of the image quality by improving the reconstruction algorithms for an inherently challenging PET radionuclide with low internal pair-production allows us to confirm tumoral deposition, detect non-target radionuclide distribution, accurately calculate post-therapy dosimetry and predict treatment efficacy. This allows advanced personalized care planning.

Aiming to increase signal to noise ratio, we developed a new algorithm LKYG for 90Y PET image reconstruction, which is featured by decreasing the number of iterations, decreasing the cutoff of the filter thickness, and increasing the number of the subsets. This approach significantly enhanced the image quality. This algorithm should be recommended for routine use of 90Y PET imaging if the hypothesis is further confirmed in a multicenter prospective study.

DISCLOSURE

No potential conflict of interest relevant to this article was reported.

PATIENT POPULATION

The institutional review board approved this study and the requirement to obtain informed consent was waived because most patients in study have passed away or were overseas.

KEY POINTS

QUESTIONS: How to improve the quality of the 90Y PET imaging by optimizing the reconstruction algorithm?

PERTINENT FINDINGS: A new 90Y PET image reconstruction algorithm that decreased the number of iterations and the cutoff of the filter thickness, and increased the number of the subsets compared to the conventional reconstruction algorithm consistently achieved the highest quality assessment score in both post-SIRT and post-PRRT 90Y PET imaging.

IMPLICATIONS: The new reconstruction algorithm has significantly improved the signal to noise ratio and therefore enhanced the diagnostic yield of 90Y PET by successfully localizing the pathologies and avoiding false positive findings.

REFERENCES

1. Liu S. The role of coordination chemistry in the development of target-specific radiopharmaceuticals. *Chem Soc Rev.* 2004;33:445-461.
2. Sangro B, Bilbao JI, Iñarrairaegui M, Rodriguez M, Garrastachu P, Martinez-Cuesta A. Treatment of hepatocellular carcinoma by radioembolization using 90Y microspheres. *Dig Dis.* 2009;27:164-169.
3. Wright CL, Zhang J, Tweedle MF, Knopp MV, Hall NC. Theranostic Imaging of Yttrium-90. *Biomed Res Int.* 2015;2015:481279.
4. Shen S, DeNardo GL, Yuan A, DeNardo DA, DeNardo SJ. Planar gamma camera imaging and quantitation of yttrium-90 bremsstrahlung. *J Nucl Med.* 1994;35:1381-1389.
5. Gates VL, Esmail AA, Marshall K, Spies S, Salem R. Internal pair production of 90Y permits hepatic localization of microspheres using routine PET: proof of concept. *J Nucl Med.* 2011;52:72-76.
6. Bagni O, D'Arienzo M, Chiaramida P, et al. 90Y-PET for the assessment of microsphere biodistribution after selective internal radiotherapy. *Nucl Med Commun.* 2012;33:198-204.
7. Kao YH, Corlett A, Jorna K, Rhodes A, Sivaratnam D. (90)Y PET for Qualitative and Quantitative Assessment of Residual Activity in Delivery Apparatus After Radioembolization. *J Nucl Med Technol.* 2021;49:178-179.
8. Pasciak AS, Bourgeois AC, McKinney JM, et al. Radioembolization and the Dynamic Role of (90)Y PET/CT. *Front Oncol.* 2014;4:38.
9. Mamawan MD, Ong SC, Senupe JM. Post-90Y radioembolization PET/CT scan with respiratory gating using time-of-flight reconstruction. *J Nucl Med Technol.* 2013;41:42.
10. Goedicke A, Berker Y Fau - Verburg FA, Verburg Fa Fau - Behrendt FF, Behrendt Ff Fau - Winz O, Winz O Fau - Mottaghy FM, Mottaghy FM. Study-parameter impact in quantitative 90-Yttrium PET imaging for radioembolization treatment monitoring and dosimetry.

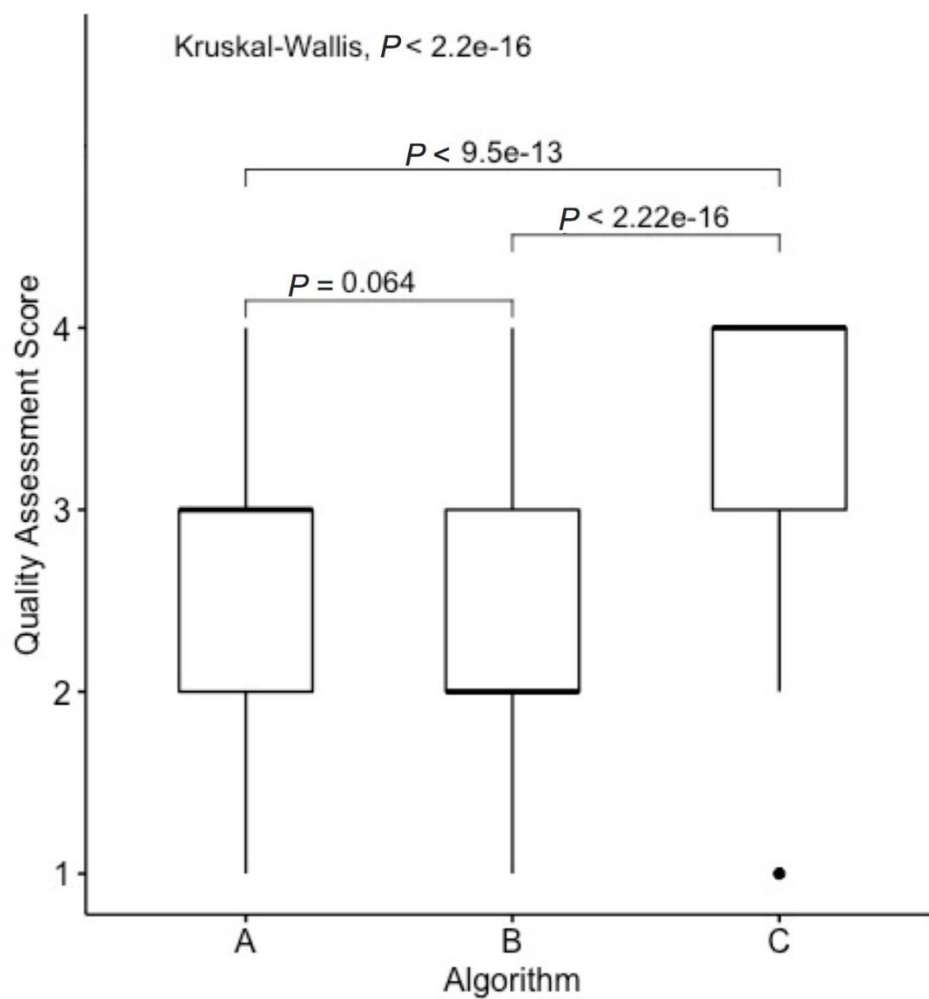


FIGURE 1. Box plots comparing median quality assessment scores between algorithms. Results from Kruskal-Wallis rank sum test and Wilcoxon rank sum test are included.

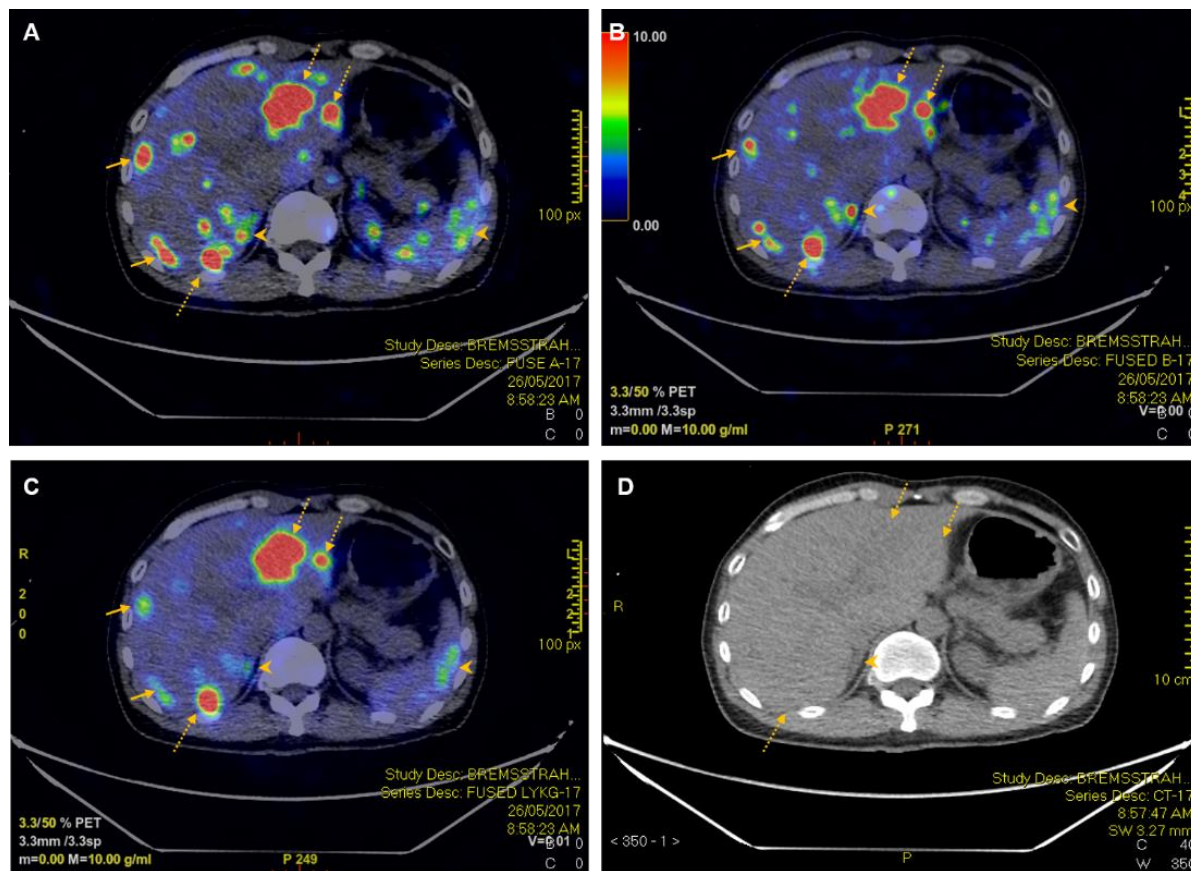


FIGURE 2. A 52-year-old gentleman with metastatic rectal neuroendocrine cancer to the liver underwent 90Y-PRRT therapy. The reconstructed PET/CT using algorithms A (Image A), B (Image B) and C (Image C) managed to detect the hepatic metastases (dotted arrows) seen on the corresponding CT images (Image D). However, there are more visible noise within the liver in both PET using Algorithms A and B compared to that of Algorithm C (solid arrows). In addition, the extrahepatic noise such as that of in the right adrenal gland and spleen (arrowheads) are less apparent using Algorithm C. Of note, the right adrenal noise can be potentially mistaken as hepatic metastasis using Algorithm A and B (arrowheads).

TABLE 1

Parameters of the three tested algorithms

Parameters	Algorithm A	Algorithm B	Algorithm C
Vue Point	HD (OSEM)	FX (OSEM + TOF)	HD (OSEM)
Gaussian Filter Cutoff	6.4mm	6.0mm	5.0mm
Number of Subsets	24	18	32
Sharp IR (PSF)	On	On	On
Z Axis Filter	Standard	Heavy	Standard
Number of Iterations	2	3	1
Matrix	192x192	192x192	192x192
Minutes / Bed	30	30	30

TABLE 2

Scoring criteria for image quality assessment

Quality Score (QS)	Rating	Description
QS-1	Non-diagnostic	Excessive noise or artefacts. Delineation of tumor and background uptake mostly impossible
QS-2	Barely diagnostic	Substantial noise and artifacts. Delineation of tumor and background uptake difficult but possible
QS-3	Fairly diagnostic	Somewhat noise and artefacts which interfere with reading. Delineation of tumor and background uptake feasible but not satisfactory
QS-4	Excellent diagnostic	No interfering noise and artefacts. Satisfactory delineation of tumor and background uptake.

TABLE 3

Patients' demographic data

Participant	Age (years)	Gender	BMI (kg/m ²)	Diagnosis	Therapy	Radiotracer Dose (GBq)
1	52	M	20.6	Rectal NET	PRRT	3.70
2	58	M	24.9	Midgut NET	PRRT	3.70
3	39	M	19.2	Paraganglioma	PRRT	4.22
4	54	F	21.8	Metastatic midgut NET to liver	PRRT	3.03
5	41	M	19.7	Metastatic pancreatic NET to liver	SIRT	2.97
6	68	M	25.9	HCC	SIRT	1.30
7	69	M	26.1	HCC	SIRT	0.58
8	59	M	29.9	HCC	SIRT	2.50
9	96	M	25.9	HCC	SIRT	0.73
10	79	F	21.4	HCC	SIRT	3.00

Abbreviations: Body mass index (BMI); Female (F), Gigabecquerel (GBq), Hepatocellular carcinoma (HCC); Male (M), neuroendocrine tumor (NET); Peptide Receptor Radionuclide Therapy (PRRT); Selective Internal Radiation Therapy (SIRT)

TABLE 4

Number and percentage of discrete scores rated by ten readers on 10 patients' scans reconstructed using Algorithms A, B and C

Algorithm	Therapy	Score 1	Score 2	Score 3	Score 4	P-value
A	SIRT	0 (0.0%)	11 (18.3%)	38 (63.3%)	11 (18.3%)	<0.001
	PRRT	10 (25.0%)	24 (60.0%)	6 (15.0%)	0 (0.0%)	
	SIRT + PRRT	10 (10.0%)	35 (35.0%)	44 (44.0%)	11 (11.0%)	
B	SIRT	0 (0.0%)	28 (46.7%)	29 (48.3%)	3 (5.0%)	<0.001
	PRRT	14 (35.0%)	13 (32.5%)	13 (32.5%)	0 (0.0%)	
	SIRT + PRRT	14 (14.0%)	41 (41.0%)	42 (42.0%)	3 (3.0%)	
C	SIRT	0 (0.0%)	0 (0.0%)	15 (25.0%)	45 (75.0%)	<0.001
	PRRT	1 (2.5%)	8 (20.0%)	24 (60.0%)	7 (17.5%)	
	SIRT + PRRT	1 (1.0%)	8 (8.0%)	39 (39.0%)	52 (52.0%)	

Abbreviations: Peptide Receptor Radionuclide Therapy (PRRT); Selective Internal Radiation Therapy (SIRT)

TABLE 5

Multivariate analysis comparing quality assessment scores

Variables		Multivariable model		
		Adjusted odds ratio	95% CI	P-value
Age	-	0.98	0.95-0.997	0.024
Gender	Male	Reference	-	-
	Female	0.83	0.44-1.58	0.576
BMI	-	0.90	0.81-0.99	0.026
Radioligand	PRRT	Reference	-	-
	SIRT	23.99	11.87-50.35	<0.001
Dose	-	0.89	0.66-1.19	0.418
Algorithm	A	Reference	-	-
	B	0.46	0.26-0.80	0.007
	C	17.4	9.16-34.15	<0.001

Abbreviations: Female (F); Male (M); Peptide Receptor Radionuclide Therapy (PRRT); Selective Internal Radiation Therapy (SIRT)